Chapter 3

STUDY OF MOLECULES RELEVANT TO PLASMA PROCESSES

In this chapter, we examined electron interactions on plasma-relevant molecules such as CF_2O,C_2F_4O, C_3F_6O, C_4F_8O, $C_5F_{10}O$, *and* $C_6F_{12}O$, *among others. These molecules are known as perfluoroketone (PFK) molecules. We present the results of elastic and inelastic (ionisation and excitation) cross section calculations for electron scattering from perfluoroketone (PFK) molecules,* $C_XF_{2X}O$ *(x = 1-6), over a broad energy range, from the ionisation potential (IP) to 5 keV. As described in Chapter 2, when analysing atomic targets, we must make very few approximations when compared to studying molecules.*

3.1 Introduction

Perfluoroketones (PFKs), $C_XF_{2X}O$ (x = 1-6), are a family of chemicals that include carbon-fluorine connected as well as a ketone component (figure 3.1). PFK substances are extensively applied in the industry, owing to their low Global Warming Potential (GWP), for instance, as a covering medium in high-voltage gadgets and as cleaning, etching, and doping gas drivers in plasma reactors [1,2] to substitute sulphur hexafluoride (SF_6), that is frequently applied as the gas protecting medium in multiple commercial electrical services due to its large insulating capability [3,4]. Because of its extended lifetime (3,200 years) across a 100-year timeline, and a high GWP figure of 23,500 in the natural environment (Fu et al., 2016; Maiss & Brenninkm,-.jer, 1998; Wu et al., 2017), SF_6 is another notable greenhouse gas. The Kyoto Protocol standards provide for a reduction in global warming gases, and hence SF_6 emissions [8]. One of the four approaches for treating SF_6 involves breakdown via plasma or electrical discharge, which results in the complete elimination of SF_6 [9]. Gases containing PFK molecules are regarded a good candidate for SF_6 in this case due to their high dielectric strength and it might be used as an insulating layer in an expensive-voltage electrical system instead.

Smaller PFK molecules, such as CF_2O and C_2F_4O, are also major byproducts of inductively linked plasma processes like Ar-CF_4-O_2 plasmas [10]. C_3F_6O's low GWP value (100) has led to its use as a standby for SF_6 in the semiconductors and display sectors for dry polishing of silica composites [11]. C_4F_8O is now utilized in Cherenkov devices as the plasma treatment gas, as a detergent for chemical vapour deposition (CVD) chambers, and in high-voltage gas insulation procedures [12,13], and has a low GWP (33% of SF_6) [12].

$C_5F_{10}O$ and $C_6F_{12}O$ have also been selected as alternatives to SF_6 because to its significant dielectric strength (E_r), strong arcs quenching capacity, low GWP, and additional uses in Gas Insulated Switchgear (GIS) and Gas Insulated Switchgear (GIS). $C_5F_{10}O$ has a dielectric strength double that of SF_6 and a GWP 1/23,900 times that of SF_6 [14]. Similarly, $C_6F_{12}O$ has a greater dielectric strength (around 2.7 times) and a GWP that is approximately $1/_{23,500}$ that of SF_6. It also has a low level of toxicity ($LC50 > 100000$ ppm) [15]. $C_6F_{12}O$ with CO_2 or air as the credential gas is now considered an acceptable substitute for SF_6 [16,17]. PFK molecules, on the other hand, can provide a viable economic and environmental alternative to SF_6.

Electron-driven ionisation of PFK compounds in plasma reactions is a crucial mechanism that initiates the swarm of electrons that decides whether the discharge can be sustained. The dielectric strength of gases is calculated using Monte Carlo computations and Boltzmann equation interpretation [18,19]. These mathematical frameworks are utilised for calculating electron swarm variables such as the effective ionisation coefficient, drift velocity, and diffusion coefficient. A comprehensive collection of electron scattering cross-sections needs to be produced in order to determine the efficacy of PFKs in industrial gas discharges, GIS, GIL, and plasma reactors.

3.2 Literature Survey Of PFK Targets

In table 3.1, we discuss all these investigations carried out. Let us review the previous

Studies of the Plasma relevant (PFK) compounds as follows:

Table 3.1 Prior research on e^- - PFK scattering processes

Target	Cross – section	Impact energy range	Reference
CF_2O	Q_{ion}	IE to 1000 eV	[2]
C_2F_4O			[2]
C_3F_6O			[2] [20]
	$Q_{ion}, Q_{inel}, \sum Q_{exc}$	IP to 5000 eV	[21]
C_4F_8O	Q_{ion}	IE to 1000 eV Threshold to 30 eV	[2] [12]
	$Q_{ion}, Q_{inel}, \sum Q_{exc}$	Threshold to 5000 eV	[21]
$C_5F_{10}O$	Q_{ion}	IE to 1000 eV Threshold to 400 eV Threshold to 2000 eV	[2] [22] [23]

	Q_{ion}, Q_{inel}, $\sum Q_{exc}$	IP to 5000 eV	[21]
$C_6F_{12}O$	Q_{ion}	Threshold to 400 eV Threshold to 2000 eV	[22] [24]
	Q_{ion}, Q_{inel}, $\sum Q_{exc}$	IP to 5000 eV	[21]

3.3 Properties Of Perfluoroketone Molecules

Table 3.2 shows the dielectric strengths and GWP of the compounds examined in relation to SF_6 for easy reference.

Table 3.2 Dielectric Strength (E_r) and GWP comparative to SF_6 of PFK compounds

Molecule	**E_r**	**GWP**
SF_6	1 [15]	23900 [16]
CF_2O	-	-
C_2F_4O	-	-
C_3F_6O	1 [25]	<100 [2]
C_4F_8O	1.2 - 1.4 [26]	8000 [12]
$C_5F_{10}O$	1.5 – 2.0 [15]	<1 [15]
$C_6F_{12}O$	2.7 [15]	1 [15]

Properties of the Plasma relevant Compounds, which are used for computations, are tabulated in table 3.3.

Table 3.3 Target properties of PFK molecules

Molecule	IP (eV)	Polarizability ($10^{-24}cm^{-3}$)
CF_2O	13.02	1.88
C_2F_4O	-	4.6
C_3F_6O	12.051	7.5
C_4F_8O	12.837	7.96
$C_5F_{10}O$	12.016	8.83
$C_6F_{12}O$	11.408	11.44

In figure 3.1, a schematics illustration of the Perfluoroketone compounds has been shown.

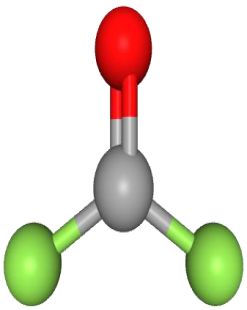

CF_2O

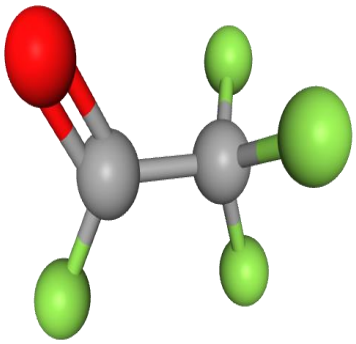

C_2F_4O

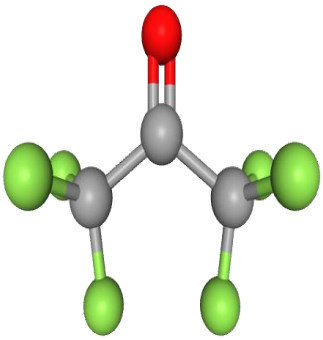

C_3F_6O

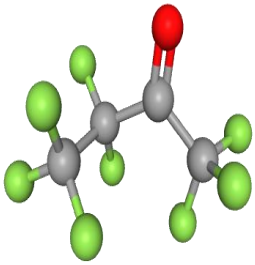

C_4F_8O

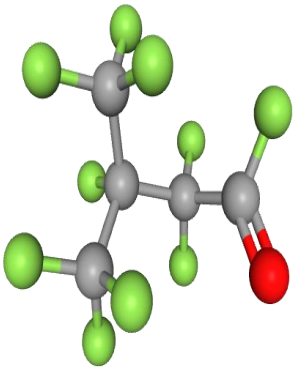

$C_5F_{10}O$

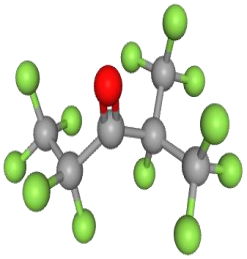

$C_6F_{12}O$

Figure 3.1 Schematic Diagrams of PFK molecules

(https://pubchem.ncbi.nlm.nih.gov)

3.4 Electron Induced Total Cross Sections For Perfluoroketone (PFK) Molecules

Here we have made a thorough study of the electron interaction with six essential plasma relevant molecules such as CF_2O, C_2F_4O, C_3F_6O, C_4F_8O, $C_5F_{10}O$ and $C_6F_{12}O$.

Present results as well as the available comparisons were divided into two groups and reported as follows:

(A) Inelastic cross sections: In this area, graphical findings from Q_{inel}, Q_{ion} and ΣQ_{exc} have been reported. Q_{ion} ionization cross sections are determined using the CSP-ic method.

(B) Total and elastic cross sections: This category contains graphical output from Q_T and Q_{el}.

3.4.1 CF_2O

(A) Inelastic cross sections

The various cross sections, which comes under the inelastic effects, are shown in figure 3.2.

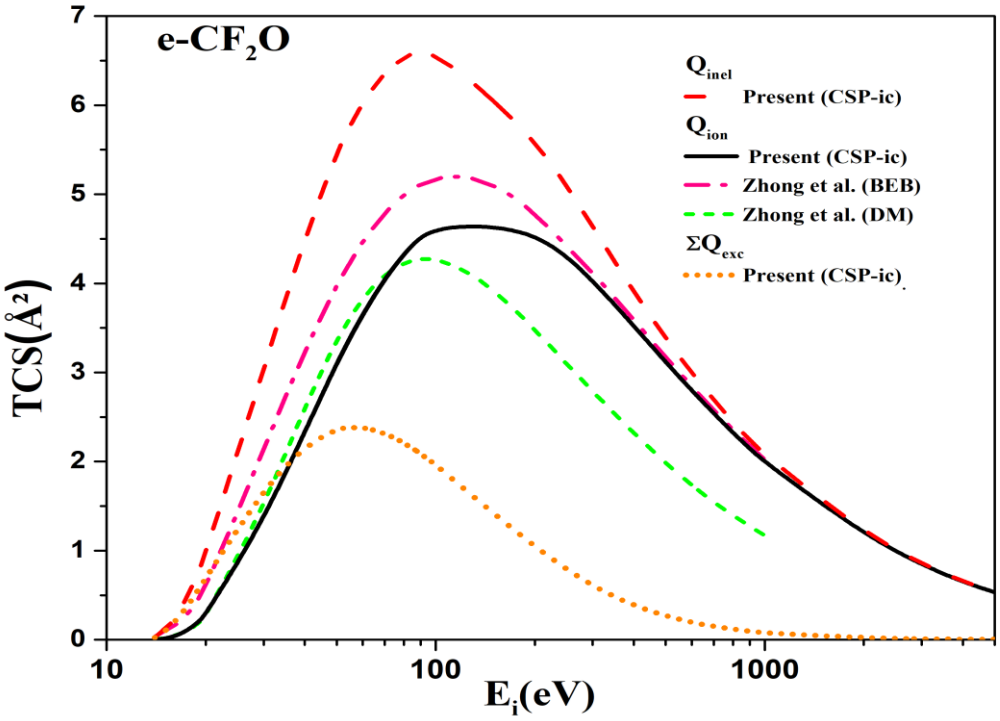

Figure 3.2 Total CS for electron impact on CF_2O

Solid: Q_{ion} (Present); Dash: Q_{inel}(Present); Dash Dot: [2] **Q_{ion} (BEB); Short Dash:** [2] **Q_{ion} (DM); Dot:Present ΣQ_{exc}**

As shown in figure 3.2, our Q_{ion} for e-CF_2O agrees well with the Q_{ion} calculated by [2] employing the BEB approach across the upper range of energy. Our Q_{ion} findings, on the other hand, grow more slowly at the threshold level and are less than the maximum BEB outcomes, but inside the specified improbability of roughly 10% for BEB findings [27–29]. While the current Q_{ion} results are greater than the Deutsch Maerk (DM) values of Zhong et al. [2], and they exclude implicit ionization as in auto-ionization, etc. above the topmost value, they coincide at energies less than 80 eV. The uppermost arc represents Q_{inel}(Present), which

includes all electronic excitations and ionization, and the bottom most is ΣQ_{exc}, which has no comparison in the literature. In figure, 3.3 elastic and total cross sections are shown and there is no comparison available for this.

(B) Total and elastic cross-sections

The various cross sections Q_T and Q_{el}, which comes under the elastic effects are shown in figure 3.3.

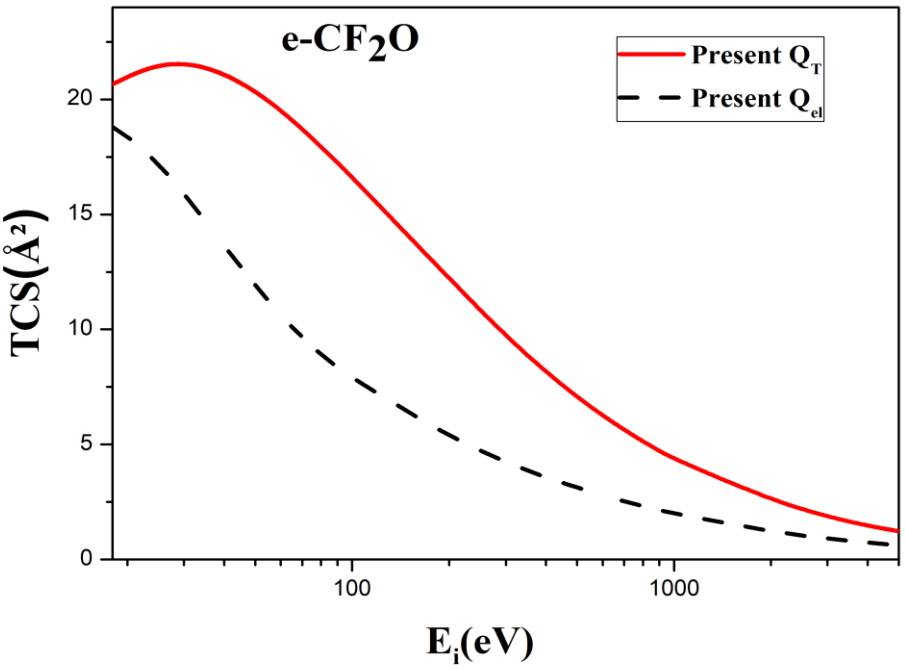

Figure 3.3 Total CS for electron -CF_2O interaction

Solid: Q_T(Present); Dashed curve: Q_{el}(Present)

Table 3.4 lists the computed TCS values for CF_2O.

Table 3.4 Total cross-sections (Å²) for CF_2O molecule.

E_i (eV)	Q_{ion}	Q_{el}	Q_T
18	0.178	18.802	20.66
20	0.38	18.373	20.969

30	1.783	15.888	21.524
40	3.065	13.642	21.068
50	4.014	11.932	20.319
60	4.683	10.637	19.505
70	5.143	9.652	18.696
80	5.424	8.923	17.942
90	5.591	8.357	17.252
100	5.683	7.878	16.628
200	5.292	5.328	12.216
300	4.492	4.216	9.712
400	3.863	3.567	8.149
500	3.39	3.117	7.062
600	3.022	2.788	6.264
700	2.731	2.527	5.637
800	2.49	2.316	5.135
900	2.289	2.141	4.722
1000	2.118	1.994	4.374
2000	1.236	1.218	2.582
3000	0.873	0.903	1.864
4000	0.671	0.732	1.471
5000	0.542	0.629	1.232

3.4.2 C_2F_4O

(A) Inelastic Cross Section

Figure 3.4 depicts the various cross sections for C_2F_4O which are subject to the inelastic effects.

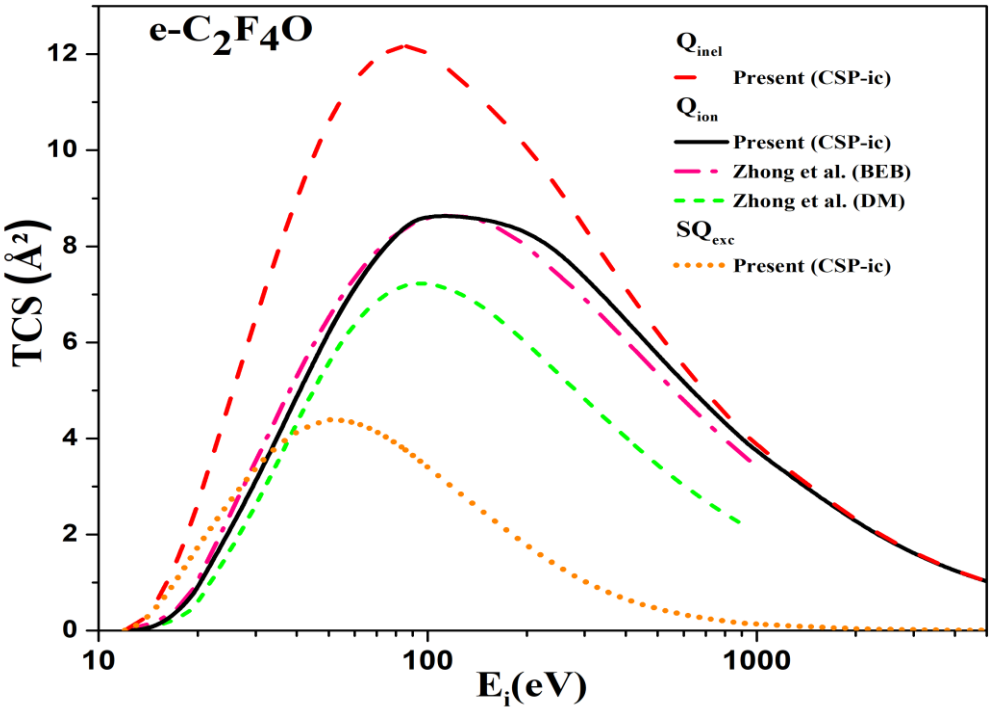

Figure 3.4 Total CS for e-C_2F_4O impact

Solid: Q_{ion}(Present); Dash: Q_{inel}(Present); Dash Dot: [2] **Q_{ion} (BEB); Short Dash:** [2] **Q_{ion} (DM); Dot: ΣQ_{exc}(Present)**

The current Q_{ion} data for e-C_2F_4O, as shown in figure 3.4, is in exceptional correspond with the BEB statistics across the complete energy spectrum [2]. Below 50 eV, the DM findings of [2] are less than existing values as well as the BEB results of [2]. For the first time, Q_{inel} and ΣQ_{exc} are computed for C_2F_4O in this work. Figure shows 3.5 elastic and total cross sections with no comparison.

(B) Total and elastic cross-sections

In figure 3.5, you can see all of the different cross sections, denoted by the notations Q_T and Q_{el} that are affected by the elastic effects.

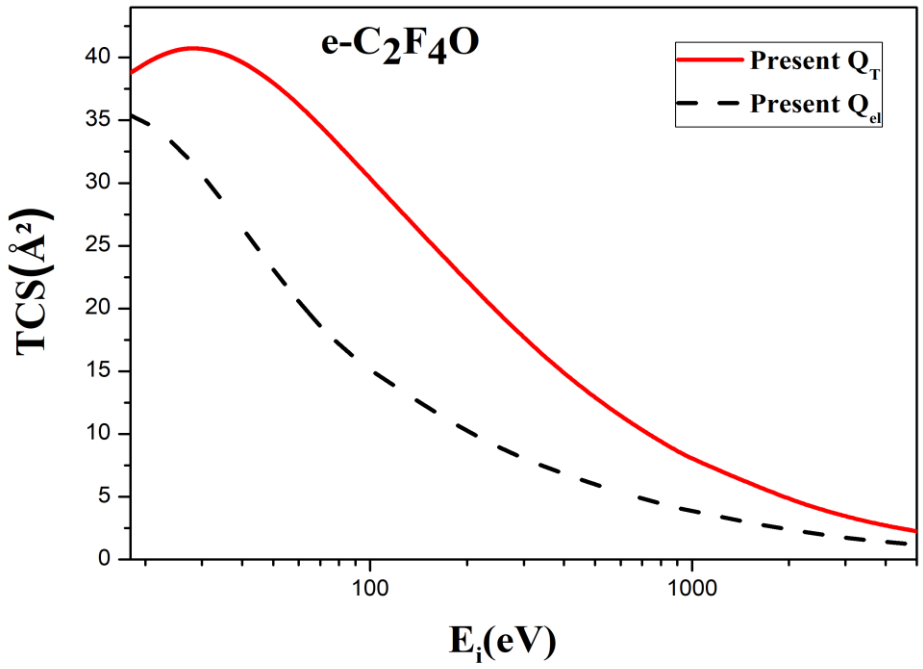

Figure 3.5 Total CS for e-C_2F_4O interaction

Solid: Q_T(Present); Dashed curve: Q_{el}(Present);

Calculated values of TCS for C_2F_4O are enumerated in table 3.5

Table 3.5 Total cross-sections (Å²) for C_2F_4O molecule.

E_i (eV)	Q_{ion}	Q_{el}	Q_T
18	0.509	35.406	38.78
20	0.882	34.831	39.517
30	3.061	30.645	40.69
40	4.887	26.447	39.618
50	6.205	23.136	37.967
60	7.129	20.582	36.232

70	7.775	18.619	34.55
80	8.219	17.157	33.011
90	8.522	16.017	31.623
100	8.719	15.051	30.384
200	8.486	10.069	22.11
300	7.383	8.015	17.632
400	6.464	6.813	14.835
500	5.747	5.971	12.882
600	5.178	5.349	11.442
700	4.712	4.852	10.305
800	4.326	4.450	9.395
900	4.002	4.114	8.643
1000	3.727	3.831	8.007
2000	2.229	2.334	4.732
3000	1.598	1.725	3.415
4000	1.242	1.395	2.693
5000	1.024	1.197	2.258

3.4.3 C_3F_6O

(A) Inelastic Cross Section

The numerous cross sections for C_3F_6O that are subject to the inelastic effects are depicted in Figure 3.6. These cross sections include Q_{inel}, Q_{ion}, and ΣQ_{exc}.

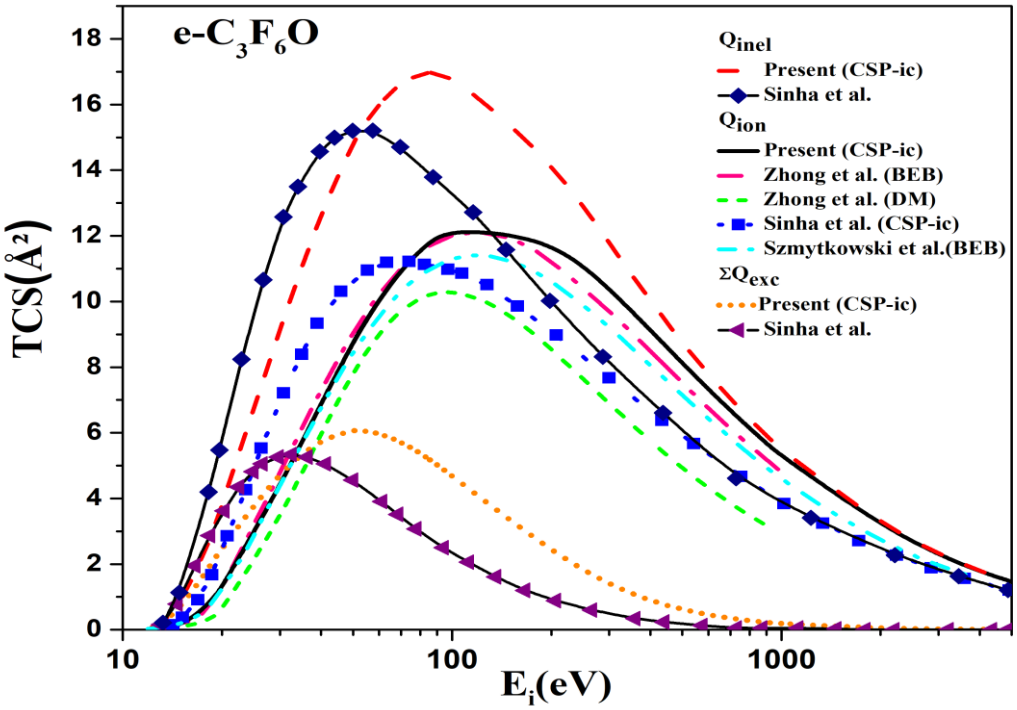

Figure 3.6 Total CS for electron impact on C_3F_6O

Solid: Q_{ion}(Present); Dash: Q_{inel}(Present); Dash Dot: [2] **Q_{ion} (BEB); Short Dash:** [2] **Q_{ion} (DM); Short Dot: ΣQ_{exc}(Present); -■- curve:** [21] **Q_{ion} (CSP-icN); Dash Dot Dot:** [20] **Q_{ion} (BEB); -♦- curve:** [21] **Q_{inel} (CSP-icN); -◄- curve:** [21] **ΣQ_{exc} (CSP-icN);**

Figure 3.6 depicts the cross-sections for scattering by electron from C_3F_6O. When we compare Q_{inel} (top most curve) with ΣQ_{exc} (bottom most curve), we see that the current data are more substantial than Sinha et al [21], and their crests are at inferior energies. Sinha et al [21] produced Q_{ion} data that is marginally lower than the current outcomes as well as BEB statistics, and their ultimate value arises at a less energy than all of the other findings. As Sinha et al [21] point out; this swing may be owing to the addition of charge of nucleus for calculation that influences the highest value and its point. Over the energy spectrum of inquiry, the current Q_{ion} are in great accord with the results of BEB computations described by Zhong et al. [2]. Beyond the peak of Q_{ion}, the DM findings are continuously lower than both the current and BEB

results [2], despite exhibiting reasonable agreement up to the peak of Q_{ion}. In figure, 3.7 Q_{el} and Q_T are graphically represented and there is no available comparison for this.

(B) Total and elastic cross sections

Figure 3.7 illustrates the numerous cross sections for C_3F_6O that are subject to the elastic effects. These cross sections include Q_{el} and Q_T.

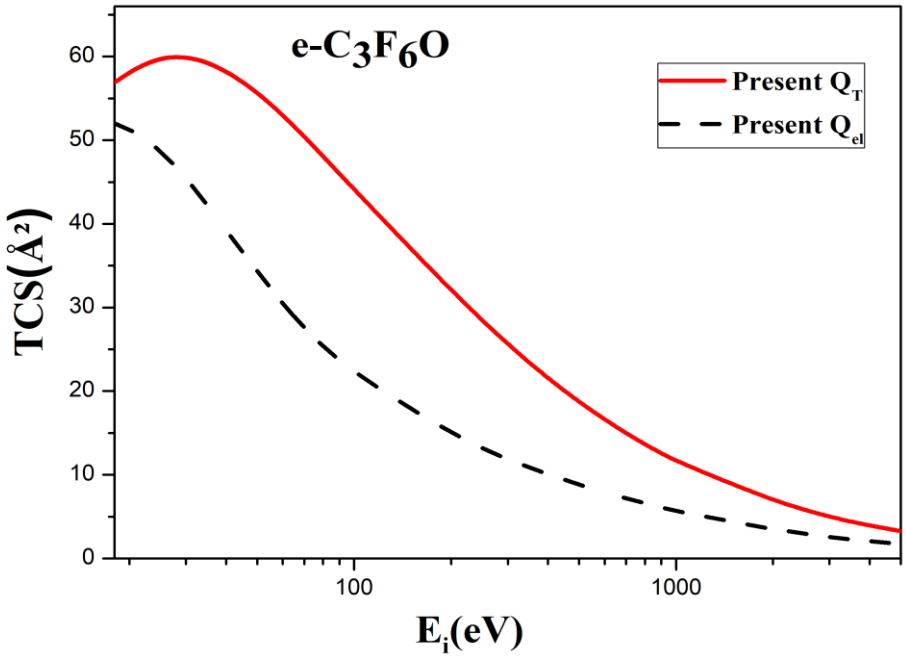

Figure 3.7 Total CS for electron C_3F_6O impact

Solid: Q_T(Present); Dashed curve: Q_{el}(Present);

Table 3.6 lists the calculated values of TCS for C_3F_6O.

Table 3.6 Total cross-sections (Å²) for C_3F_6O molecule.

E_i (eV)	Q_{ion}	Q_{el}	Q_T
18	0.758	52.010	56.900
20	1.291	51.289	58.065

30	4.356	45.402	59.856
40	6.904	39.252	58.168
50	8.738	34.340	55.615
60	10.023	30.527	52.959
70	10.919	27.586	50.404
80	11.537	25.391	48.080
90	11.958	23.677	45.994
100	12.232	22.224	44.14
200	11.936	14.810	32.004
300	10.406	11.814	25.552
400	9.124	10.059	21.521
500	8.125	8.825	18.702
600	7.330	7.910	16.620
700	6.679	7.177	14.973
800	6.142	6.584	13.655
900	5.684	6.087	12.564
1000	5.294	5.668	11.64
2000	3.184	3.45	6.882
3000	2.285	2.547	4.966
4000	1.779	2.058	3.915
5000	1.464	1.765	3.284

3.4.4 C_4F_8O

(A) Inelastic Cross Section

Figure 3.8 illustrates the multiple cross sections for C_4F_8O that are affected by the inelastic effects. These cross sections are subject to the effects. These transverse sections are denoted by the letters Q_{inel}, Q_{ion}, and ΣQ_{exc}.

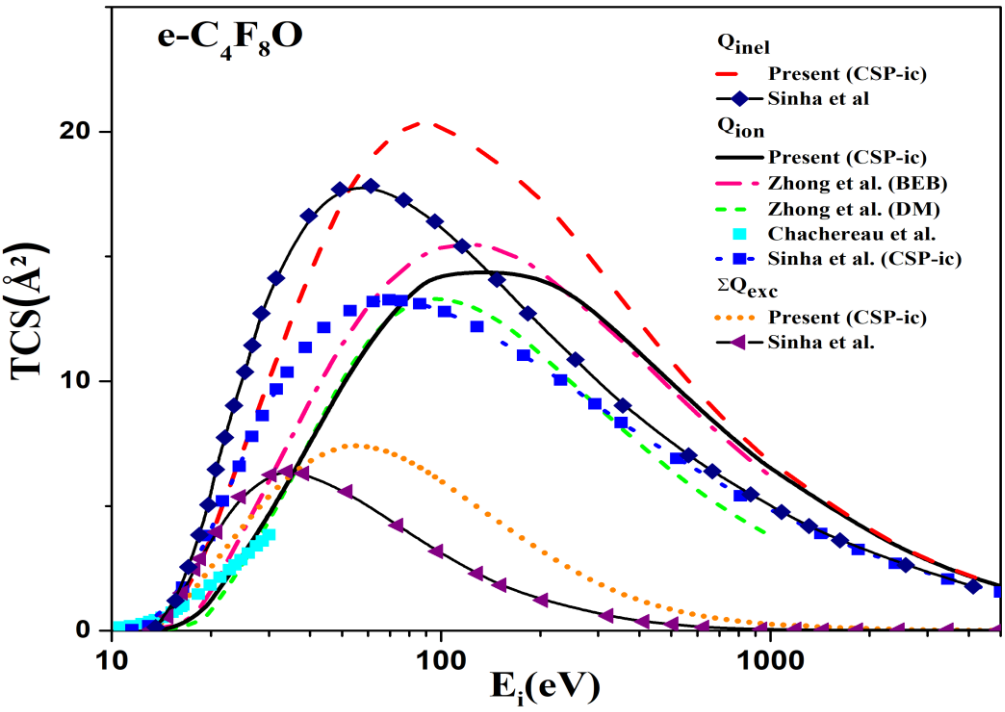

Figure 3.8 Inelastic processes for C_4F_8O

Solid: Q_{ion}(Present); Dash: Q_{inel}(Present); Dash Dot: [2] **Q_{ion} (BEB); Short Dash:** [2] **Q_{ion} (DM); Dot: ΣQ_{exc}(Present) ; ■** [12] **Q_{ion}; -■- curve:** [21] **Q_{ion} (CSP-icN); -♦- curve:** [21] **Q_{inel} (CSP-icN); -◄- curve:** [21] **ΣQ_{exc} (CSP-icN);**

As demonstrated in figure 3.5, a similar scenario for e-C_4F_8O is obtained for current Q_{inel}, Q_{ion}, and ΣQ_{exc} in comparison to the results of Sinha et al [21]. The current Q_{ion} values correlate well with calculated by Zhong et al. by means of the BEB technique [2]. Beyond the peak of Q_{ion}, the current findings and BEB outcomes are once again higher to those produced applying the DM approach, although the current evidence is consistent at low energies. The current statistics also agrees well with the only prototype investigation, Chachereau et al. [12],

which was only accessible for low energies (30 eV). Figure depicts 3.9 Q_{el} and Q_T visually, with no accessible comparison.

(B) Total and elastic cross-sections

Figure 3.9 is an illustration of the various cross sections for C_4F_8O that are subject to the effects of elastic deformation. These are denoted by the letters Q_{el} and Q_T.

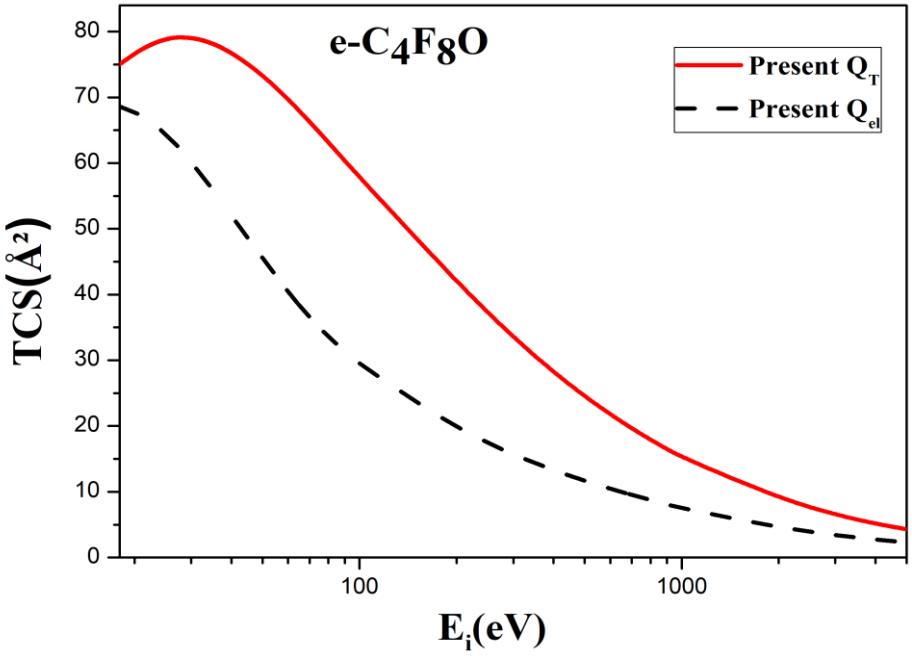

Figure 3.9 Elastic Processes for C_4F_8O

Solid: Q_T(Present); Dashed curve: Q_{el}(Present);

Table 3.7 lists the computed TCS values for C_4F_8O.

Table 3.7 Total cross-sections (Å²) for C_4F_8O molecule

E_i (eV)	Q_{ion}	Q_{el}	Q_T
18	0.625	68.614	75.02
20	1.161	67.747	76.613
30	4.549	60.159	79.022

40	7.554	52.057	76.718
50	9.799	45.544	73.263
60	11.413	40.472	69.686
70	12.573	36.553	66.258
80	13.401	33.625	63.149
90	13.985	31.337	60.365
100	14.383	29.397	57.896
200	14.436	19.551	41.898
300	12.685	15.613	33.472
400	11.149	13.305	28.207
500	9.948	11.679	24.522
600	8.98	10.471	21.798
700	8.186	9.502	19.641
800	7.528	8.718	17.915
900	6.977	8.06	16.485
1000	6.495	7.505	15.273
2000	3.912	4.566	9.032
3000	2.804	3.369	6.517
4000	2.183	2.721	5.137
5000	1.792	2.333	4.31

3.4.5 $C_5F_{10}O$

(A) Inelastic Cross Section

The numerous cross sections for $C_5F_{10}O$ that are influenced by the inelastic effects are depicted in Figure 3.10 for your reference. These different cross sections are affected by the effects. The letters Q_{inel}, Q_{ion}, and ΣQ_{exc} are used to indicate these transverse sections.

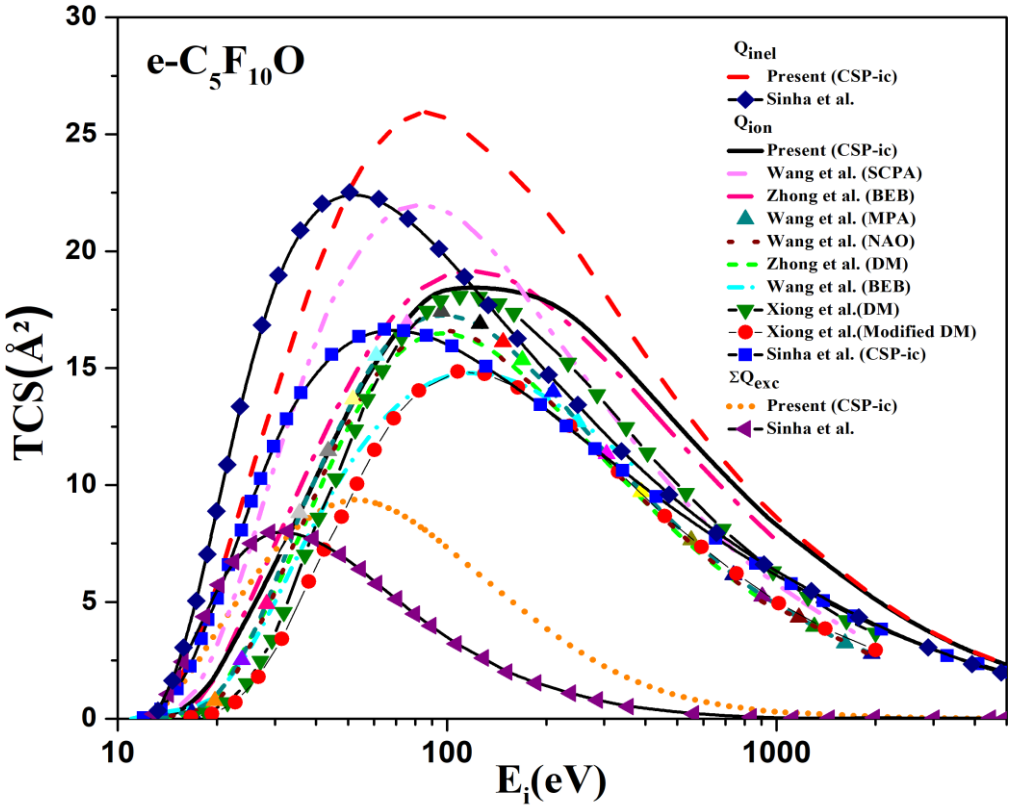

Figure 3.10 Inelastic interaction processes for $C_5F_{10}O$

Solid: Q_{ion}(Present); Dash: Q_{inel}(Present); Dash Dot: [2] **Q_{ion} (BEB); Short Dash:** [2] **Q_{ion} (DM); Short Dot: ΣQ_{exc}(Present); Dash Dot Dot:** [24] **Q_{ion} (SCPA); -▲- curve:** [24] **Q_{ion} (MPA); Dot:** [24] **Q_{ion} (NAO); Short Dash Dot:** [22] **Q_{ion} (BEB); -▼- curve:** [23] **Q_{ion} (DM); -●- curve:** [23] **Q_{ion} (Modified DM); -■- curve:** [21] **Q_{ion} (CSP-icN); -♦- curve:** [21] **Q_{inel} (CSP-icN); -◄- curve:** [21] **ΣQ_{exc} (CSP-icN);**

In figure 3.10, the current Q_{inel} and ΣQ_{exc} for $C_5F_{10}O$ are compared to Sinha et al [21], and we see comparable behaviour as previously mentioned. Throughout the energy range, the current Q_{ion} are in great accord with cross-sections calculated by Zhong et al. [2] using the BEB technique (IP - 5000 eV). Beyond the peak of Q_{ion}, the DM approach results are systematically lower than the current and BEB findings [2]. Wang et al. published Q_{ion}'s BEB findings. [22] underperform the current results and the BEB outcomes of Zhong et al [2]. The current Q_{ion} are in decent accordance with the findings given by Wang et al. [24] for low energies, i.e. below Q_{ion}, utilising MPA (Mulliken Population Analysis) and NAO (Natural Atomic Orbital) methodologies (peak). However, the results of Wang et al. [24] utilizing the SCPA approach grossly underestimate all Q_{ion} effects. The current findings are also consistent

obtained by Xiong et al. [23] by means of the DM approach, but their Modified DM outcomes [23] it seems that undervalued cross-sections. The current findings, as well as the BEB outcomes of Zhong et al [2], overstate the statistics of Sinha et al [21], with the topmost point of Sinha et al [21] occurring at a lower energy. Elastic processes (Q_{el} and Q_T) are shown in figure 3.11 with no accessible comparison data.

(B) Total and elastic cross sections

Figure 3.11 depicts Q_{el} and Q_T for $C_5F_{10}O$, which accounts for the substance's elastic effects**.**

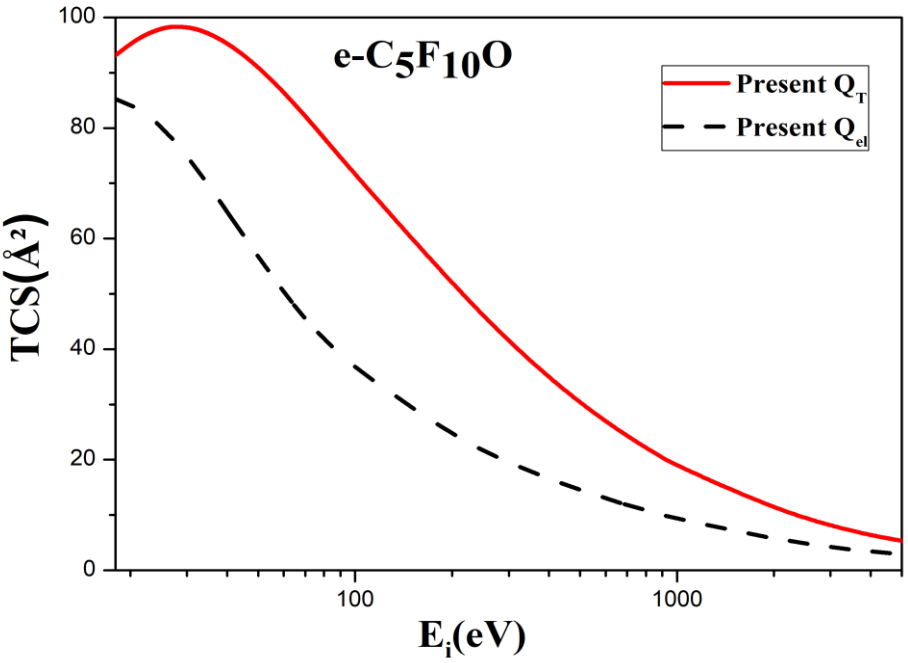

Figure 3.11 Elastic interaction CSs for $C_5F_{10}O$

Solid: Q_T(Present); Dashed curve: Q_{el}(Present);

Table 3.8 lists the calculated TCS values for $C_5F_{10}O$.

Table 3.8 Total cross-sections ($Å^2$) for $C_5F_{10}O$ molecule

E_i (eV)	Q_{ion}	Q_{el}	Q_T
18	1.124	85.218	93.14
20	1.918	84.205	95.161

30	6.505	74.916	98.188
40	10.348	64.862	95.268
50	13.133	56.748	90.911
60	15.111	50.417	86.413
70	16.496	45.52	82.112
80	17.464	41.859	78.218
90	18.125	38.997	74.736
100	18.574	36.57	71.652
200	18.305	24.292	51.792
300	16.042	19.412	41.392
400	14.106	16.551	34.893
500	12.591	14.533	30.342
600	11.379	13.032	26.976
700	10.388	11.827	24.309
800	9.567	10.852	22.175
900	8.863	10.033	20.406
1000	8.264	9.342	18.906
2000	5	5.682	11.182
3000	3.595	4.191	8.068
4000	2.801	3.384	6.359
5000	2.307	2.901	5.336

3.4.6 $C_6F_{12}O$

(A) Inelastic Cross Section

Figure 3.12 depicts Q_{inel}, Q_{ion}, and Q_{exc} for $C_6F_{12}O$. These cross sections take into account all inelastic effects**.**

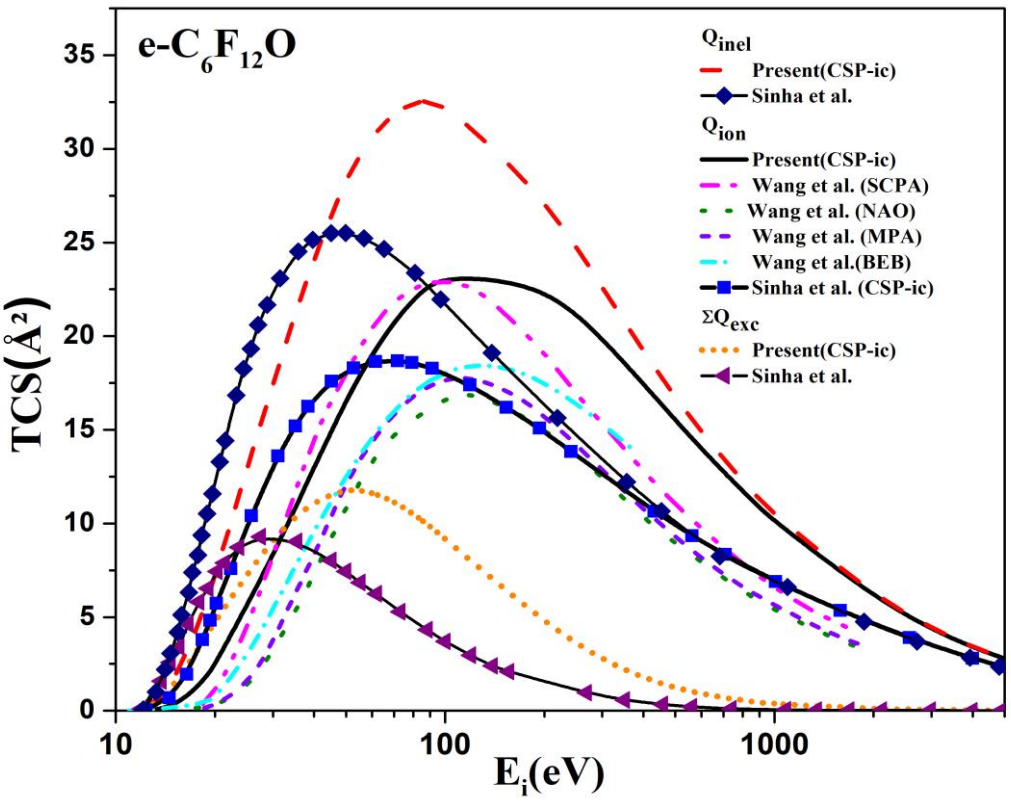

Figure 3.12 Inelastic processes for $C_6F_{12}O$

Solid: Q_{ion}(Present); Dash: Q_{inel}(Present); Short Dot: ΣQ_{exc}(Present) ; Dash Dot Dot: [24] **Q_{ion} (SCPA); Short Dash:** [24] **Q_{ion} (MPA); Dot:** [24] **Q_{ion} (NAO); Short Dash Dot:** [22] **Q_{ion} (BEB);-■- curve:** [21] **Q_{ion} (CSP-icN); -♦- curve:** [21] **Q_{inel} (CSP-icN); -◄- curve:** [21] **ΣQ_{exc} (CSP-icN);**

As demonstrated in figure 3.12, e- $C_6F_{12}O$ exhibits close similarity to that stated before for present Q_{inel}, Q_{ion}, and ΣQ_{exc} in comparison to the results of Sinha et al [21]. The current Q_{ion} show rather strong agreement on outcomes offered by Wang et al. [24] applying the SCPA approach for energies as far as the Q_{ion} peak, after that the current data likely to be larger than Wang et al. (SCPA) [24]. The current Q_{ion} results are also better than those obtained by Wang et al. [24] utilising NAO and MPA methodologies. Wang et al [22] described BEB findings

for Q_{ion} that are lower than our outcomes on a consistent basis. Nonetheless, the point of the Q_{ion} (peak) is the identical for the current and Wang et al [22] BEB data. Figure 3.13 shows Q_{el} and Q_T graphically.

(B) Total and elastic cross-sections

Figure 3.13 displays the Q_{el} and Q_T values for $C_6F_{12}O$. This section accounts for all elastic effects.

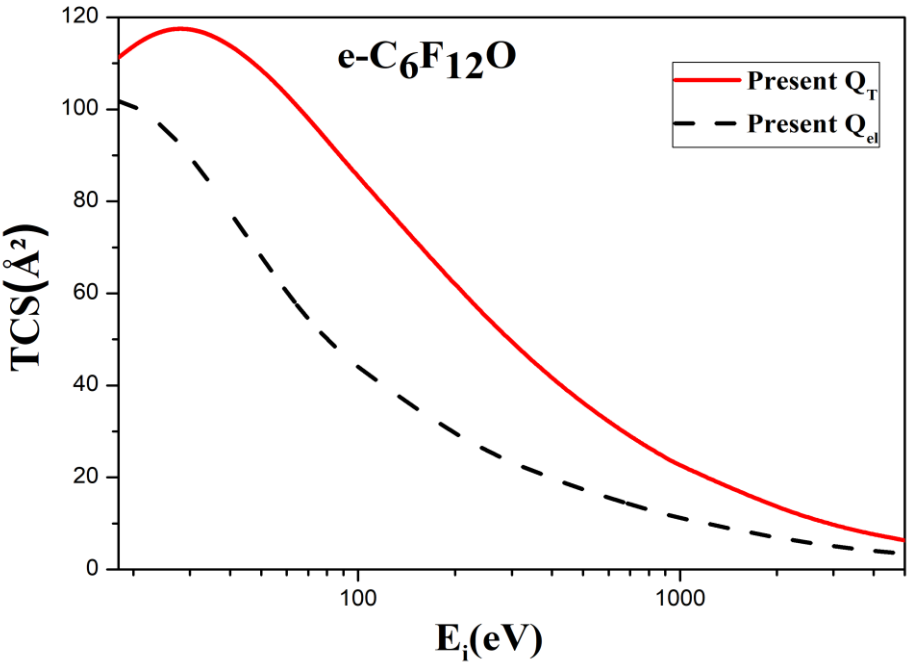

Figure 3.13 Elastic processes for $C_6F_{12}O$

Solid: Q_T(Present); Dashed curve: Q_{el}(Present);

Table 3.9 lists the calculated TCS values for $C_6F_{12}O$.

Table 3.9 Total cross-sections (Å²) for $C_6F_{12}O$ molecule.

E_i (eV)	Q_{ion}	Q_{el}	Q_T
18	1.439	101.822	111.26
20	2.444	100.663	113.709

30	8.214	89.673	117.354
40	13.03	77.667	113.818
50	16.512	67.952	108.559
60	18.979	60.362	103.14
70	20.706	54.487	97.966
80	21.906	50.093	93.287
90	22.723	46.657	89.107
100	23.274	43.743	85.408
200	22.801	29.033	61.686
300	19.893	23.211	49.312
400	17.444	19.797	41.579
500	15.533	17.387	36.162
600	14.01	15.593	32.154
700	12.769	14.152	28.977
800	11.74	12.986	26.435
900	10.863	12.006	24.327
1000	10.115	11.179	22.539
2000	6.074	6.798	13.332
3000	4.354	5.013	9.619
4000	3.384	4.047	7.581
5000	2.782	3.469	6.362

3.5 Estimated Cross Sections And Polarizability Forecast

Table 3.10 lists various target parameters as well as the expected polarizability of three molecules, C_2F_4O, $C_5F_{10}O$, and $C_6F_{12}O$. The molecule's number of electrons (N) determines the dimension of the molecular cloud.

Table 3.10 Present Molecule's properties and projected polarizability

N	**Target**	**IP (eV)**	**Polarizability ($10^{-24}cm^{-3}$)**		
			Available	**Predicted**	**found through www.chemspider.com**
32	CF_2O	13.89 [2]	1.88 (www.cccbdb.gov.in)	--	2.8
56	C_2F_4O	12.84 [2]	--	4.21	4.6 (deviation 8.4 %)
80	C_3F_6O	12.05 [2]	5.62 [14], 7.5 [21]	--	6.7
104	C_4F_8O	12.84 [2]	7.47 [14], 7.96 [21]	--	8.6
128	$C_5F_{10}O$	12.02 [2]	8.83 [21]	9.84	10.6 (deviation 7.1%)
152	$C_6F_{12}O$	11.41 [30]	11.44 [21]	12.54	12.6 (deviation 0.4 %)

Figure 3.14 shows total ionization cross sections for all the target studied in this chapter. Which gives clear idea about TICS rises as number of electron increases.

In figure 3.14, total Q_{ion} for all the present PFK targets are shown graphically up to 5000eV. Figure 3.14 depicts this property by plotting the Q_{ion} of all compounds. The magnitudes of these cross-sections rise with the dimension of the charge cloud for a given impact energy

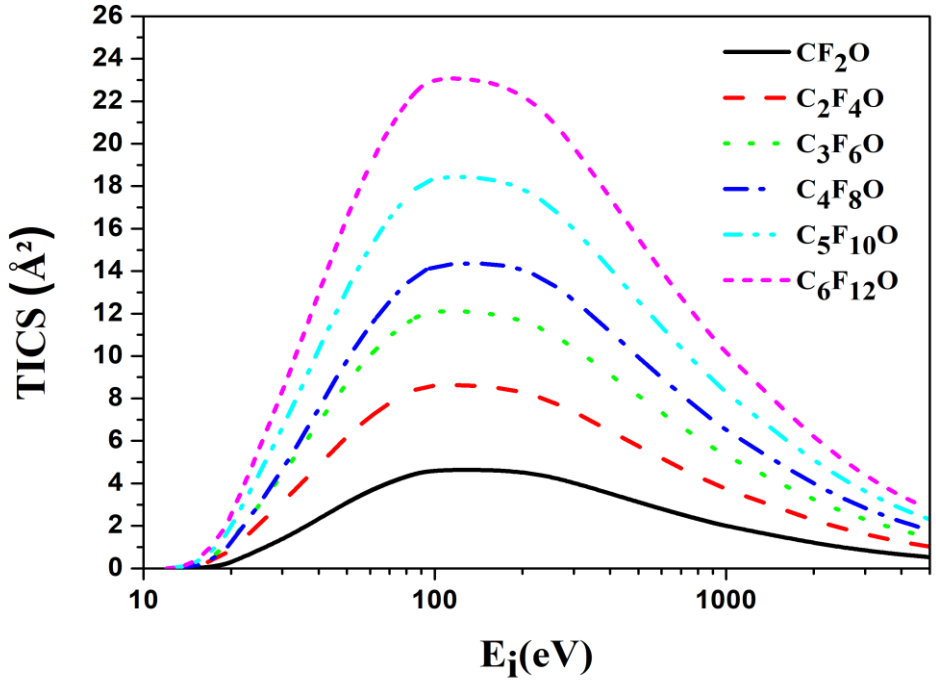

Figure 3.14 Q_{ion}(Present) for e-$C_XF_{2X}O$ (X=1-6) collision

The SCOP formalism designates the electron impact with the molecular cloud of charge and provides for a measureable assessment of the likelihood of numerous electron-sponsored molecular events.

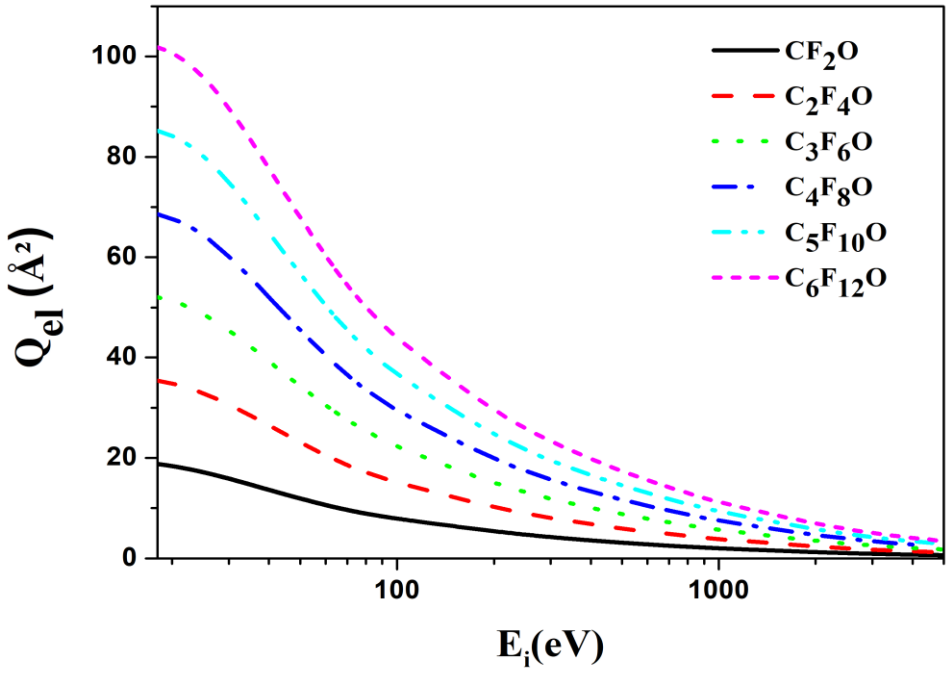

Figure 3.15 Q_{el}(Present) for e-$C_XF_{2X}O$ (X=1-6) collision

As a result, it is reactive to cloud size via the N (number of electrons) of the target molecule. Like figure 3.14, a similar pattern may be seen in figures 3.15 and 3.16, which depict Q_{el} and Q_T, correspondingly.

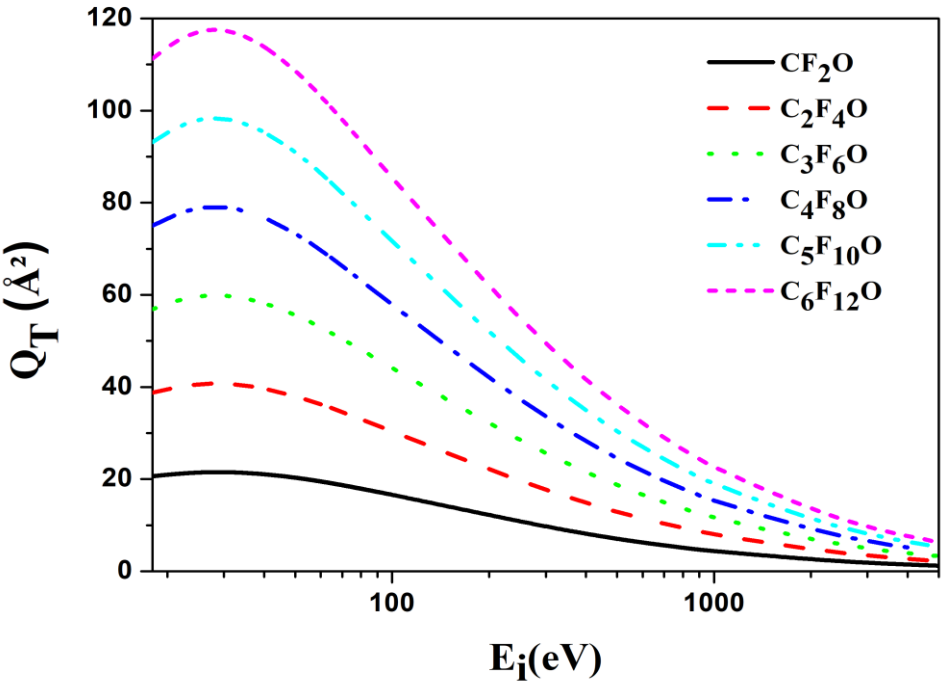

Figure 3.16 Q_T(Present) for e-$C_XF_{2X}O$ (X= 1-6) collision

Apart from the dimension of the atomic cloud, Q_{ion} are subtle to the ionization potential that does not deviate significantly for these massive atoms (table 3.6). As a result, the peaks of Q_{ion} have a linear relationship with N. (figure 3.17). It shows the minor difference in IPs of CF_2O and $C_6F_{12}O$. Because of the slightly greater IP, the point for CF_2O is below the line, whereas the point for $C_6F_{12}O$ is above the line (table 3.6).

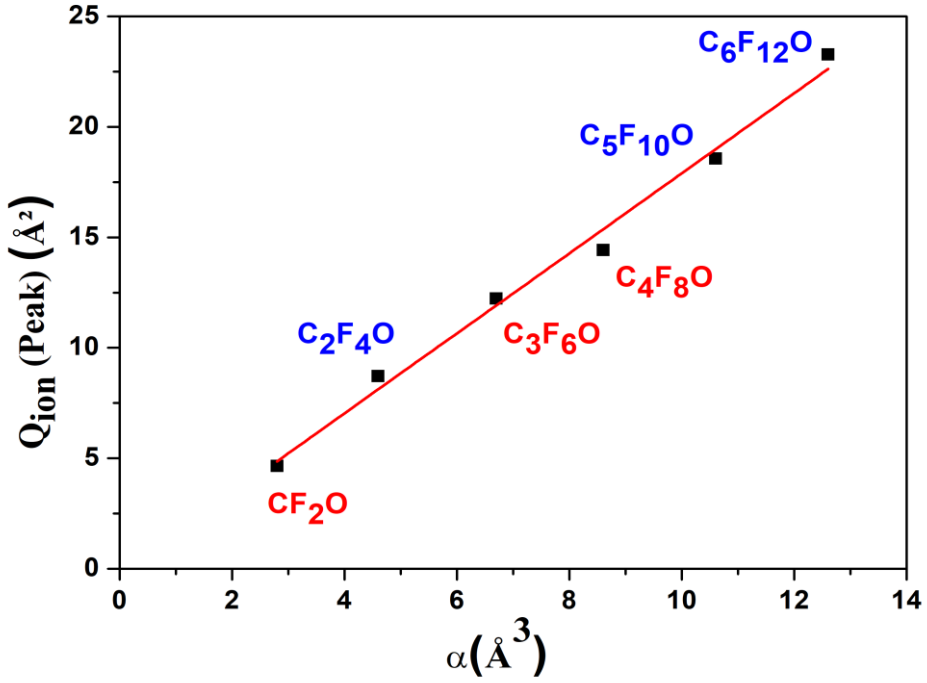

Figure 3.17 Relationship between Q_{ion} (Peak) and α (polarizability)

We also found a linear association between Q_{ion} (peak) and α, (figure 3.17) and $\sqrt{\frac{\alpha}{I_p}}$ (figure 3.18), as proposed by Bart et al. [31].

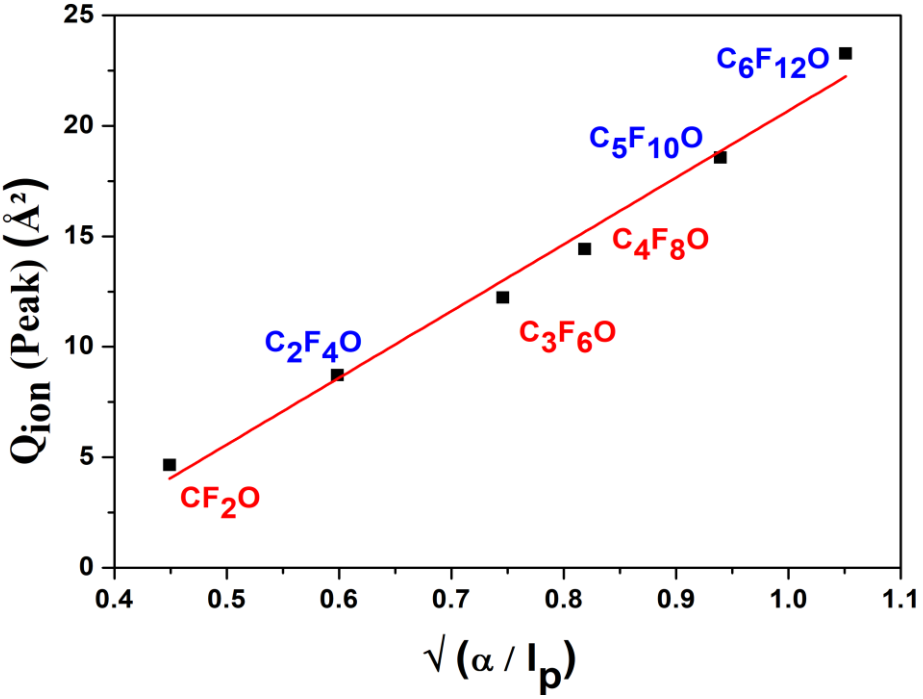

Figure 3.18 Relationship between Q_{ion} (Peak) and $\sqrt{\alpha/I_p}$

Because of the spherical approximation and semi-empirical character of Q_{ion} assessment, the blending of SCOP and CSP-ic makes it possible to compute total cross-sections for a large number of complicated compounds using the identical methods with a modest improbability of roughly 10%. We show the significance of different TCS calculated in this effort over e-C_3F_6O at Ep=90 eV. (figure 3.19).

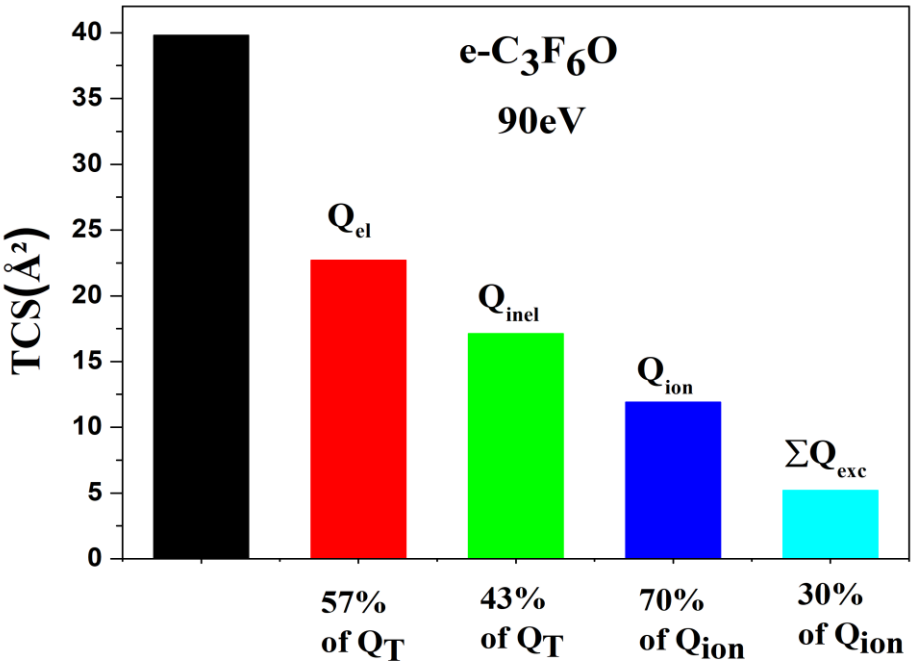

Figure 3.19 Relative Total CS

Whereas Q_T is the top bound for electron-induced events, Q_{el} represents 57% of Q_T and Q_{inel} represents 43% of Q_T. However, as Joachain [32] points out, Q_{el} should be equal to Q_{inel} at E_p, the tiny variation in the current situation is due to the theory's approximations. As projected, Q_{ion} contributes 70% of Q_{inel} and ΣQ_{exc} contribute 30% of Q_{inel}.

All of these applicable quantities are computed solely within the quantum environment. This adds dependability and stability to the data and verifies the concept's resilience.

3.6 Chapter Summary

We conducted a thorough theoretical investigation of electron scattering from perfluoroketone (PFK) molecules, $C_XF_{2X}O$ ($X = 1-6$), spanning a large range of energy from the molecular

ionization potential to 5 keV. The SCOP technique was used to estimate total elastic (Q_{el}), total inelastic (Q_{inel}), and total cross sections (Q_T), and the CSP-ic approach was used to calculate total ionization (Q_{ion}), and the summed total excitation cross sections (ΣQ_{exc}). In the supplemental data, the computed findings are shown graphically (figs. 3.2-3.13) as well as statistically. We discovered that the estimated Q_{ion} agrees well with the published BEB statistics [2,33] and frequently with the SCPA data of Wang et al. [24], but while the DM results [2] are prone to correspond well with energies of 70 - 80 eV for $C_XF_{2X}O$ ($X = 1 - 4$), these cross sections are generally smaller than the findings we have acquired.

We discovered that the total number of electrons, N, correlates with the dimension of the molecular cloud and that the TCSs grow with the amount of target's electron (figure 3.14-3.16). We investigated the sensitivity of Q_{ion} to the ionization potential, IP, and discovered a linear relationship between Q_{ion} (peak) and N in the lack of significant unorthodoxy in IP for these compounds (figure 3.17). We additionally, found a linear relationship among Q_{ion} (peak) and IP and α (figure 3.17-3.18), as expected by Bart et al [31]. We projected the dipole polarizability of $C_XF_{2X}O$ (x = 2, 5, 6) using these correlation analyses and discovered that our estimated polarizabilities are in great accordance with those figured using the internet freeware www.chemspider.com.

This is the debut study to report ΣQ_{exc} and Q_{inel} for CF_2O and C_2F_4O, as well as Q_{el} and Q_T for all of these vital ecological and plasma pertinent compounds, whose exceptionally truncated global warming potential (GWP) and increased dielectric strength make them appealing prospects for industrial usage. We hope that this effort will inspire other theorists and experimentalists to do similar research.

3.7 Bibliography

[1] S. KESARI, F. E. BEHR, M. G. COSTELLO, R. M. FLYNN, R. M. MINDAY, J. G. OWENS, and D. R. VITCAK, *USE OF PERFLUOROKETONES AS VAPOR REACTOR CLEANING, ETCHING, AND DOPING GASES*, (2002).

[2] L. Zhong, J. Wang, X. Wang, and M. Rong, *Calculation of Electron-Impact Ionization Cross Sections of Perfluoroketone (PFK) Molecules CxF2xO (x = 1–5) Based on Binary-Encounter-Bethe (BEB) and Deutsch-Märk (DM) Methods*, Plasma Sources Sci Technol **27**, 095005 (2018).

[3] J. Tang, X. Rao, B. Tang, X. Liu, X. Gong, F. Zeng, and Q. Yao, *Investigation on SF6 Spark Decomposition Characteristics under Different Pressures*, IEEE Transactions on Dielectrics and Electrical Insulation **24**, 2066 (2017).

[4] C. T. Dervos, P. Vassiliou, and J. A. Mergos, *Thermal Stability of SF6 Associated with Metallic Conductors Incorporated in Gas Insulated Switchgear Power Substations*, J Phys D Appl Phys **40**, 6942 (2007).

[5] M. Maiss and C. A. M. Brenninkmeijer, *Atmospheric SF6: Trends, Sources, and Prospects*, Environ Sci Technol **32**, 3077 (1998).

[6] Y. Fu, X. Wang, X. Li, A. Yang, G. Han, Y. Lu, Y. Wu, and M. Rong, *Theoretical Study of the Decomposition Pathways and Products of C5- Perfluorinated Ketone (C5 PFK)*, AIP Adv **6**, (2016).

[7] Y. Wu, C. Wang, H. Sun, M. Rong, A. B. Murphy, T. Li, J. Zhong, Z. Chen, F. Yang, and C. Niu, *Evaluation of SF6-Alternative Gas C5-PFK Based on Arc Extinguishing Performance and Electric Strength*, J Phys D Appl Phys **50**, 385202 (2017).

[8] S. 1966- Oberthür and H. E. 1961- Ott, *The Kyoto-Protocol* (2000).

[9] J. Zhang, J. Z. Zhou, Q. Liu, G. Qian, and Z. P. Xu, *Efficient Removal of Sulfur Hexafluoride (SF6) through Reacting with Recycled Electroplating Sludge*, Environ Sci Technol **47**, 6493 (2013).

[10] K. Furuya, A. Ide, H. Okumura, and A. Harata, *Mass Spectrometric Investigation and Formation Mechanisms of High-Mass Species in the Downstream Region of Ar/CF4/O2 Plasmas*, Physical Chemistry Chemical Physics **11**, 934 (2009).

[11] I. J. Kim, H. K. Moon, J. H. Lee, N. E. Lee, J. W. Jung, and S. H. Cho, *Silicon Nitride Etch Characteristics in SF6/O2 and C3F6O/O2 Plasmas and Evaluation of Their Global Warming Effects*, Microelectronics Reliability **52**, 2970 (2012).

[12] A. Chachereau, J. Fedor, R. Janečková, J. Kočišek, M. Rabie, and C. M. Franck, *Electron Attachment Properties of C-C4F8O in Different Environments*, J Phys D Appl Phys **49**, 375201 (2016).

[13] K. J. Kim, C. H. Oh, N.-E. Lee, J. H. Kim, J. W. Bae, G. Y. Yeom, and S. S. Yoon, *Global Warming Gas Emission during Plasma Cleaning Process of Silicon Nitride Using C-C4F8O/O2 Chemistry with Additive Ar and N2*, Journal of Vacuum Science & Technology B: Microelectronics and Nanometer Structures Processing, Measurement, and Phenomena **22**, 483 (2004).

[14] L. Zhong, M. Rong, X. Wang, J. Wu, G. Han, G. Han, Y. Lu, A. Yang, and Y. Wu, *Compositions, Thermodynamic Properties, and Transport Coefficients of High-Temperature C5F10O Mixed with CO2 and O2 as Substitutes for SF6 to Reduce Global Warming Potential*, AIP Adv **7**, (2017).

[15] M. Rabie and C. M. Franck, *Assessment of Eco-Friendly Gases for Electrical Insulation to Replace the Most Potent Industrial Greenhouse Gas SF6*, Environ Sci Technol **52**, 369 (2018).

[16] J. D. Mantilla, N. Gariboldi, S. Grob, and M. Claessens, *Investigation of the Insulation Performance of a New Gas Mixture with Extremely Low GWP*, EIC 2014 - Proceedings of the 32nd Electrical Insulation Conference 469 (2014).

[17] G. T. Linteris, V. I. Babushok, P. B. Sunderland, F. Takahashi, V. R. Katta, and O. Meier, *Unwanted Combustion Enhancement by C6F12O Fire Suppressant*, Proceedings of the Combustion Institute **34**, 2683 (2013).

[18] M. Vinodkumar, H. Bhutadia, C. Limbachiya, and K. N. Joshipura, *Electron Impact Total Ionization Cross Sections for H2S, PH3, HCHO and HCOOH*, Int J Mass Spectrom **308**, 35 (2011).

[19] K. N. Joshipura, B. G. Vaishnav, and C. G. Limbachiya, *Ionization and Excitation of Some Atomic Targets and Metal Oxides by Electron Impact*, Pramana - Journal of Physics **66**, 403 (2006).

[20] C. Szmytkowski, P. Moejko, and E. Ptasińska-Denga, *Electron Scattering from Hexafluoroacetone Molecules: Cross Section Measurements and Calculations*, Journal of Physics B: Atomic, Molecular and Optical Physics **44**, 205202 (2011).

[21] N. Sinha, V. M. Patel, and B. Antony, *Ionization Cross Sections for Plasma Relevant Molecules*, Journal of Physics B: Atomic, Molecular and Optical Physics **53**, 145101 (2020).

[22] F. Wang, Q. Dun, S. Chen, L. Zhong, X. Fan, and L. L. Li, *Calculations of Total Electron Impact Ionization Cross Sections for Fluoroketone and Fluoronitrile*, IEEE Transactions on Dielectrics and Electrical Insulation **26**, 1693 (2019).

[23] J. Xiong, X. Li, J. Wu, X. Guo, and H. Zhao, *Calculations of Total Electron-Impact Ionization Cross Sections for Fluoroketone C5F10O and Fluoronitrile C4F7N Using Modified Deutsch–Märk Formula*, J Phys D Appl Phys **50**, 445206 (2017).

[24] Y. Wang, S. Tian, X. Zhang, W. Liu, Y. Wang, and G. Zhang, *Theoretical Calculation of Total Electron-Impact Ionization Cross Section of C6F12O*, AIP Adv **10**, (2020).

[25] X. Yu, H. Hou, and B. Wang, *Prediction on Dielectric Strength and Boiling Point of Gaseous Molecules for Replacement of SF6*, J Comput Chem **38**, 721 (2017).

[26] Z. Gao, Y. Wang, S. Wang, R. Peng, W. Zhou, P. Yu, and Y. Luo, *Investigation of Synthesis and Dielectric Properties of C-C4F8O with Its CO2/N2 Mixtures as SF6 Alternatives in Gas-Insulated Applications*, IEEE Access **8**, 3007 (2020).

[27] C. Limbachiya, M. Vinodkumar, M. Swadia, and A. Barot, *Electron Impact Total Cross Section Calculations for CH 3SH (Methanethiol) from Threshold to 5 KeV*, Mol Phys **112**, 101 (2014).

[28] Y. K. Kim and P. M. Stone, *Ionization of Boron, Aluminum, Gallium, and Indium by Electron Impact*, Phys Rev A **64**, 11 (2001).

[29] Y. K. Kim and J. P. Desclaux, *Ionization of Carbon, Nitrogen, and Oxygen by Electron Impact*, Phys Rev A **66**, 127081 (2002).

[30] X. Zhang, S. Tian, S. Xiao, Z. Deng, Y. Li, and J. Tang, *Insulation Strength and Decomposition Characteristics of a C6F12O and N2 Gas Mixture*, Energies (Basel) **10**, (2017).

[31] M. Bart, P. W. Harland, J. E. Hudson, and C. Vallance, *Absolute Total Electron Impact Ionization Cross-Sections for Perfluorinated Hydrocarbons and Small Halocarbons*, Physical Chemistry Chemical Physics **3**, 800 (2001).

[32] C. J. (Charles J. Joachain, *Quantum Collision Theory*, 710 (1975).

[33] M. Vinodkumar, C. Limbachiya, A. Barot, and N. Mason, *Computation of Electron-Impact Rotationally Elastic Total Cross Sections for Methanol over an Extensive Range of Impact Energy (0.1 - 2000 EV)*, Phys Rev A **87**, 012702 (2013).